Supplemental Material: Scaling of sub-gap excitations in a superconductor-semiconductor nanowire quantum dot

Eduardo J. H. Lee[1],* Xiaocheng Jiang[2], Rok Žitko[3], Ramón Aguado[4], Charles M. Lieber[2], and Silvano De Franceschi[1†]
[1] *SPSMS, CEA-INAC/UJF-Grenoble 1, 17 rue des Martyrs, 38054 Grenoble Cedex 9, France*
[2] *Harvard University, Department of Chemistry and Chemical Biology, Cambridge, MA, 02138, USA*
[3] *Jožef Stefan Institute, Jamova 39, SI-1000, Ljubljana, Slovenia and*
[4] *Instituto de Ciencia de Materiales de Madrid (ICMM), Consejo Superior de Investigaciones Científicas (CSIC), Sor Juana Inés de la Cruz 3, 28049 Madrid, Spain*

MODEL

The minimal model to treat a single quantum dot coupled to a metal reservoir is the Anderson model,

$$H = \sum_{k\sigma} \epsilon_k c^\dagger_{k\sigma} c_{k\sigma} + \epsilon_0 n + U/2(n-1)^2 + V \sum_{k\sigma} d^\dagger_\sigma c_{k\sigma} + \text{H.c.} \quad (1)$$

Here ϵ_k is the dispersion of the c electrons in the reservoir. The impurity state is denoted as d: ϵ_0 is its energy level, $n = \sum_\sigma d^\dagger_\sigma d_\sigma$ is the level occupancy, U is the Coulomb electron-electron repulsion, and V is the hybridization amplitude. If the reservoir is superconducting, there is an additional pairing term $\Delta \sum_k c_{k\uparrow} c_{-k\downarrow} + \text{H.c.}$. The hybridization strength is quantified through $\Gamma = \pi\rho V^2$, where ρ is the reservoir density of states for $\Delta = 0$. In this work, this model is extended by including two reservoirs, one normal-state and one superconducting with hybridization strengths Γ_N and Γ_S, respectively. We also include a Zeeman term $g\mu_B B S_z$, where g is the g-factor, μ_B is the Bohr magneton, B is the external magnetic field, and $S_z = (1/2)(d^\dagger_\uparrow d_\uparrow - d^\dagger_\downarrow d_\downarrow)$.

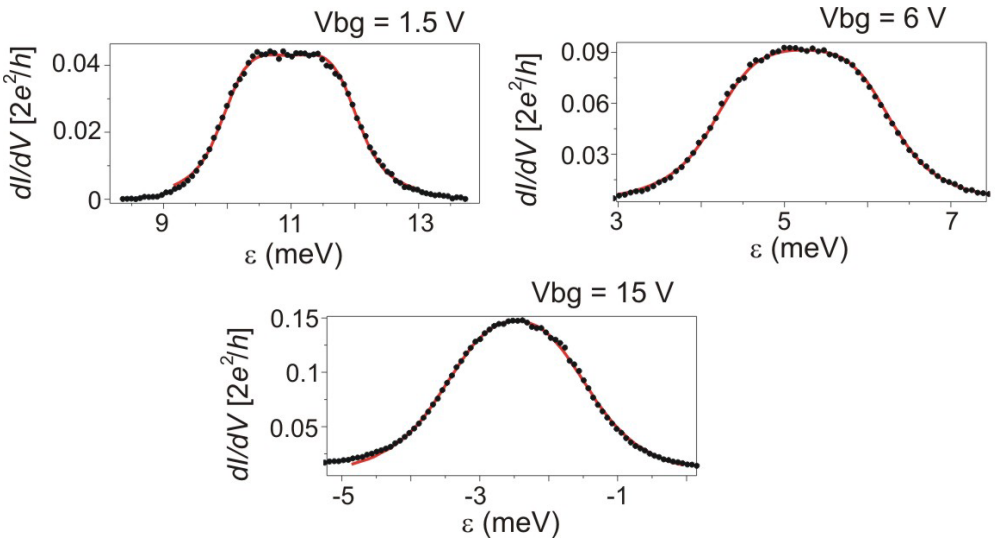

FIG. 1. Linear conductance, $dI/dV(V = 0)$, as a function of the energy level position, ϵ, taken at different values of the back gate voltage ($V_{bg} = 1.5$, 6 and 15 V). The experimental data (black dots) corresponds to device 1 (discussed in the main text). ϵ was obtained by multiplying the plunger gate voltage with the lever arm, $\alpha \approx 0.0453$. The red lines are fits performed using numerical renormalization group calculations.

* Current address: Condensed Matter Physics Center (IFIMAC), Universidad Autónoma de Madrid, 28049 Madrid, Spain.; eduardo.lee@uam.es
† silvano.defranceschi@cea.fr

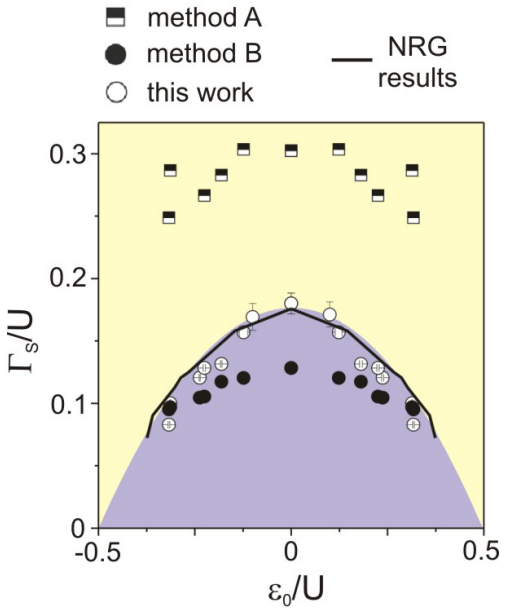

FIG. 2. Comparison of different methodologies employed to estimate device parameters. The open dots correspond to data points obtained with the methodology discussed in this work. This dataset shows excellent quantitative agreement with the phase boundary calculated by NRG (black line). By contrast, methods A and B (see text for further details) show pronounced discrepancies. The colored limits of the singlet and doublet states in the phase diagram are guides to the eye.

NORMAL STATE DATA AND ESTIMATION OF DEVICE PARAMETERS

We extracted the device parameters from the normal state linear conductance data, $dI/dV(V=0,V_{pg})$, measured at $B_\perp = 30$ mT. Before describing our methodology in further detail, we note that we have explored alternative, commonly employed methods to estimate the tunnel coupling of the dot to N and S leads, $\Gamma_{N(S)}$, namely (i) fitting the even occupancy part of normal state $dI/dV(V=0,Vpg)$ traces with Lorentzian curves [1, 2] (method A), and (ii) evaluating $\Gamma_{N(S)}$ from the height and the half width at half maximum (HWHM) of the zero-bias Kondo resonances [3] (method B). We have however verified that neither of the above methods is able to yield reliable device parameters. In order to overcome this problem, we have employed NRG to accurately compute the linear conductance G on a fine four-dimensional grid of total hybridization strengths Γ, impurity levels ϵ_0, temperatures T, and Zeeman energies E_Z, all rescaled by the interaction U. These calculations were performed in a wide parameter range, covering all experimentally relevant cases. We then fixed the Zeeman energy and the temperature, which are also held constant in the experiment. The fits of the conductance as a function of the plunger gate voltage $V_{\rm pg}$ were performed for each value of the back gate voltage $V_{\rm bg}$ separately. Specifically, for each value of V_{bg} we took of order 100 experimental data points of the $G(V_{pg})$ curve in the range $G_{\rm max}/G_{\rm min} \gtrsim 5$, discarding the low-conductance tails which typically exhibit non-universal behavior and are asymmetric. This provided the results for the position of the particle-hole symmetric point, the total hybridization $\Gamma = \Gamma_S + \Gamma_N$, the interaction U, as well as the maximum conductance which contains information about the ratio of the hybridizations for both contacts, Γ_S/Γ_N. We then calculated the sum of the coefficients of determination R^2 for the set of regressions for the different $V_{\rm bg}$, and slightly varied the Zeeman energy and the temperature to maximize this sum; this additional iterative procedure was performed to remove the uncertainty due to the experimental errors in determining the g-factor and the effective temperature of the electron gas. Very good overlap was thereby obtained for all values of $V_{\rm bg}$ simultaneously (Fig. 1, see also Fig. 2a in the main text). Through maximing R^2 we find that the effective electron temperature is 32 mK and that the Zeeman energy is not less than $E_Z = 10$ μeV, which corresponds to $g \geq 5.75$ knowing that $B_\perp = 30$ mT; further increasing E_Z did not increase the quality of the fits.

The extracted values of Γ_S, Γ_S/Γ_N, U and the Kondo temperature, T_K, for device 1 are listed in Table 1. To underscore the reliability of the methodology employed in this work, we plot the singlet-doublet phase boundaries obtained by using Γ_S/U values estimated by the alternative methods discussed above (Fig. 2). Both methods A and B yield pronounced discrepancies with respect to the data points obtained by our procedure and to the results of the NRG calculations.

Finally, we note that previous work has employed a similar approach, albeit using a different many-body method

V_{bg} (V)	Γ_S/U	U (meV)	Γ_S/Γ_U	T_K (mK)
-4.5	0.07222	2.50753	121.92	31.58
-1.5	0.0904	2.33457	104.85	95.02
0.75	0.1125	2.31231	94.38	254.5
1.5	0.1206	2.23428	85.98	327.54
3	0.12496	2.26679	74.77	383.95
6	0.15356	2.18159	41.07	803.045
9	0.1758	2.14117	33.42	1247.49
15	0.26431	1.9835	25.03	3761.59
22.5	0.33782	1.95634	21.49	6079.83

TABLE I. Parameters from device 1 extracted by fitting the experimental data using NRG.

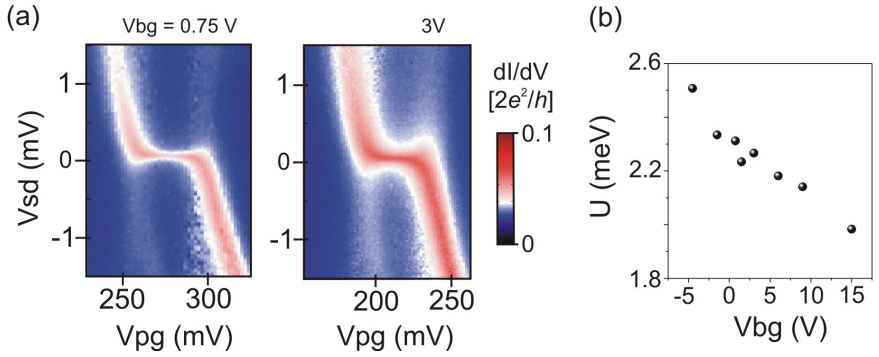

FIG. 3. (a) Normal state charge stability diagrams measured at $V_{bg} = 0.75$ and 3 V. The enhanced coupling of the quantum dot to the S lead at $V_{bg} = 3$ V manifests itself as a broader zero-bias Kondo resonance. (b) Back gate voltage dependence of the charging energy.

(namely quantum Monte Carlo), to reliably extract the device parameters of QD-based Josephson junctions [4, 5].

DEVICE 2

In this section, we discuss device 2 in further detail. In analogy to device 1, we have studied the impact of the back gate voltage on the Andreev levels of the second device. Fig. 3a displays the corresponding series of dI/dV vs. (V, V_{pg}) plots measured at different V_{bg}. In this case, the QD-S system is found in the singlet ground state for negative V_{bg}, implying a strong coupling of the dot to the S lead. As V_{bg} is tuned to 1.5 V, a quantum phase transition to the doublet ground state occurs at the center of the Coulomb diamond, as evidenced by the crossing of Andreev levels. The doublet stable region further grows as V_{bg} increases. The above observations suggest that, differently than device 1, the QD-S tunnel coupling of device 2 decreases with increasing V_{bg}. Such a hypothesis is corroborated by the back gate dependence of the Kondo temperature (shown in Fig. 3b), which was estimated from the width of the zero-bias Kondo resonances measured in the normal state.

WIDTH OF SUB-GAP RESONANCES

In this section, we discuss the width of the measured sub-gap resonances. Andreev levels at $T = 0$ are δ- functions, and thus have zero width. In an experimental setup however, the measured resonances are affected by thermal broadening and by the (weak) coupling to the normal metal tunnel probe. To elucidate the dominant broadening mechanism in our experiment, we have quantified the mean sub-gap peak width associated with each of the measurements taken at different V_{bg}. Specifically, we have performed Lorentzian fits to the sub-gap resonances and estimated the mean width using data points around the particle-hole symmetry point, as the fitting becomes less reliable near Andreev level crossings. In Fig. S4, the resulting mean peak width is plotted against Γ_N, where the error bars represent the standard deviation. The minimum peak width in our experiment is ≈ 30 μV, which is excessive to be ascribed only to thermal broadening, considering the electron temperature $T_{el} \approx 32$ mK estimated from the NRG fits. For $\Gamma_N \gtrsim 10\mu$eV, the mean peak width increases with Γ_N, suggesting that the level broadening becomes dominated by

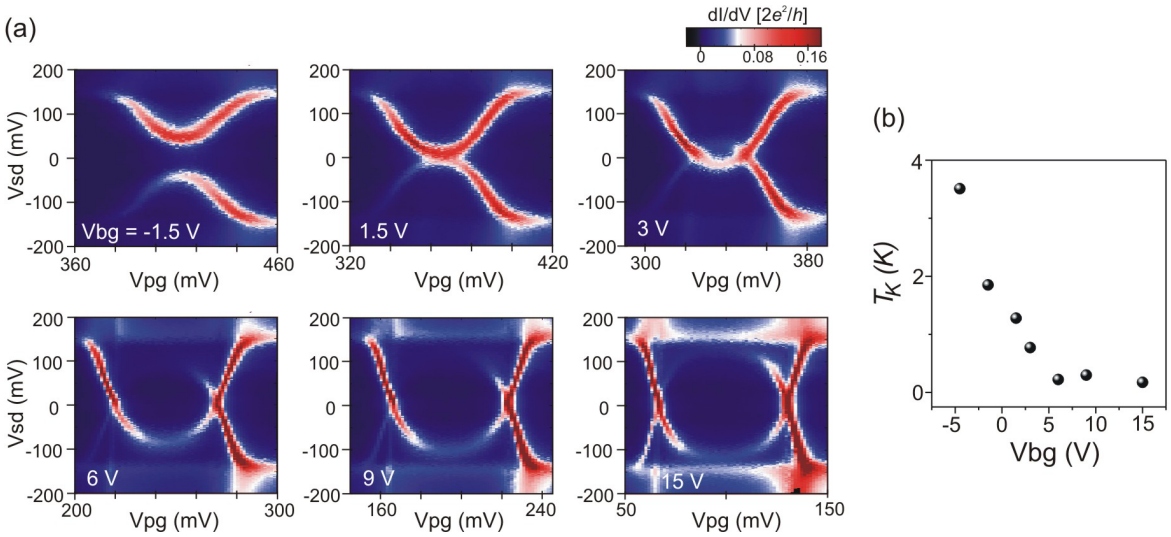

FIG. 4. (a) Series of dI/dV vs. (V, V_{pg}) plots depicting the back gate voltage dependence of Andreev levels in device 2. (b) Kondo temperature of device 2 as a function of V_{bg}. Contrary to device 1, the tunnel coupling of the quantum dot to the S lead decreases with increasing V_{bg}.

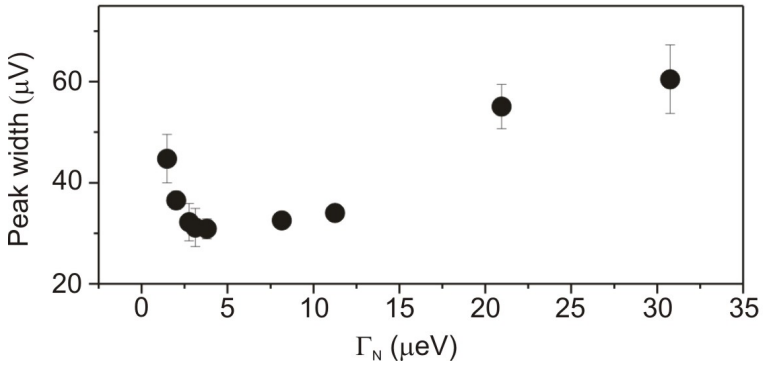

FIG. 5. Mean peak width, estimated from Lorentzian fits to the sub-gap resonances, as a function of the tunnel coupling to the normal metal probe, Γ_N. The mean value was obtained from the distribution of widths extracted from measurements taken at different V_{pg}, for a given V_{bg} (see text for further details). The error bars represent the standard deviation.

the coupling to the tunnel probe. Surprisingly, the peak width dependence experiences an upturn for weak tunnel couplings, whose origin we currently do not understand.

As a final note, we underscore that a direct comparison, in this context, between experimental and theoretical results is not possible, as the latter have been calculated at $T = 0$ yielding Andreev levels with zero width. The NRG spectral functions were later artificially broadened to reproduce the experimental data.

[1] H. I. Jorgensen, T. Novotny, K. Grove-Rasmussen, K. Flensberg, and P. E. Lindelof, Nano Lett. **7**, 2441 (2007).
[2] R. S. Deacon, Y. Tanaka, A. Oiwa, R. Sakano, K. Yoshida, K. Shibata, K. Hirakawa, and S. Tarucha, Phys. Rev. Lett. **104**, 076805 (2010).
[3] R. Maurand, T. Meng, E. Bonet, S. Florens, L. Marty, and W. Wernsdorfer, Phys. Rev. X **2**, 011009 (2012).
[4] D. J. Luitz, F. F. Assaad, T. Novotny, C. Karrasch, and V. Meden, Phys. Rev. Lett. **108**, 227001 (2012).
[5] R. Delagrange, D. J. Luitz, R. Weil, A. Kasumov, V. Meden, H. Bouchiat, and R. Deblock, Phys. Rev. B **91**, 241401 (2015).